Journal of the Korean Nuclear Society
Volume 27, Number 4, August 1995

Numerical Determination of Lateral Loss Coefficients for Subchannel Analysis in Nuclear Fuel Bundles

Sin Kim and Goon Cherl Park
Seoul National University
(Received December 27, 1994)

핵연료집합체 부수로 해석을 위한 횡방향 압력손실계수의 수치적 결정

김 신 · 박군철
서울대학교
(1994. 12. 27 접수)

Abstract

An accurate prediction of cross-flow based on detailed knowledge of the velocity field in subchannels of a nuclear fuel assembly is of importance in nuclear fuel performance analysis. In this study, the low-Reynolds number k-ε turbulence model has been adopted in two adjacent subchannels with cross-flow. The secondary flow is accurately estimated by the anisotropic algebraic Reynolds stress model. This model was numerically calculated by the finite element method and has been verified successfully through comparison with existing experimental data. Finally, with the numerical analysis of the velocity field in such subchannel domain, an analytical correlation of the lateral loss coefficient is obtained to predict the cross-flow rate in subchannel analysis codes. The correlation is expressed as a function of the ratio of the lateral flow velocity to the donor subchannel axial velocity, recipient channel Reynolds number and pitch-to-diameter.

요 약

핵연료집합체 부수로 유동장에 대한 상세한 정보에 기초해 교차류를 정확히 예측하는 것은 핵연료의 성능을 해석하는데 중요한 요소이다. 본 연구에서는 저-Reynolds 수 k-ε 난류모형을 채택하여 인접한 두 부수로 사이에 발생하는 교차류를 해석하였다. 또한, 2차유동을 정확히 모사하기 위해서 비등방성 대수응력모형을 사용하였다. 이상의 난류 모형은 유한요소법을 통해 해석되었으며 가용한 실험자료와 비교하여 검증하였다. 그리고, 부수로 유동장에 대한 수치해석 결과를 이용하여 횡방향 압력손실계수의 상관식을 구성하였다. 상관식은 교차류를 제공하는 부수로의 축방향 속도에 대한 교차류의 속도비, 제공받는 부수로의 Reynolds 수 그리고 Pitch-to-diameter의 함수로 구성되었다.

1. Introduction

In the design and safety analysis of nuclear reactors, it is very important to verify that DNBR does not exceed the safety limit. For this purpose, accurate subchannel analysis for nuclear fuel rod bundles is required. However, the thermal-hydraulic phenomena in such geometries as rod bundles are complex due to geometrical complexity and high turbulence. Also, between subchannels in the rod bundle, there exist the interchanges of physical quantities such as mass, momentum and energy. Especially, the cross-flow can induce fuel rod vibrations through vortex shedding or turbulent mechanisms. Therefore, to accurately predict the nuclear fuel performance, the knowledge on such interchanges including the turbulent effects is essential.

Coolant mixing between subchannels in rod bundles is classified into four mechanisms as follows[1]: (1) turbulent interchange, (2) diversion cross-flow, (3) flow scattering, and (4) flow sweeping. The first two mechanisms are natural mixing effects which always occur in rod bundles and the last two are forced mixing effects due to mechanical means. Turbulent interchange is natural eddy diffusion between subchannels which can be characterized by eddy diffusivities. Diversion cross-flow is a directed flow between subchannels caused by radial pressure gradients between adjacent subchannels. Flow scattering and sweeping are non-directional mixing associated with the presence of grid spacers and directed cross-flow due to mixing vanes on grid spacers, respectively.

One of the important intersubchannel interaction is the mass transfer by diversion cross-flow, which is due to the lateral pressure difference. The diversion cross-flow carries the momentum and energy and thus affects the velocity and temperature profiles in the rod bundle. This quantity is calculated in commercial computer codes with the lateral pressure loss coefficient, which correlates the cross-flow rate with the lateral pressure difference.

In COBRA-II code, the lateral pressure loss coefficient was evaluated on the basis of frictional resistance which would be observed for given lateral flow velocities in the absence of an axial flow component. This approach does not agree with the data for lateral flow through orifices in the presence of substantial axial flows. Hence, Weisman[2] pointed out that the analysis of the lateral flow between two rod bundles should recognize the strong inertial effect of axial flow on the lateral flow. Thus, using the subchannel approach, he derived the expression for the lateral pressure loss coefficient between assemblies and established a correlation using experimental data. His correlation indicates that the inertial effect is the main parameter in describing lateral pressure losses and the frictional losses are negligible.

Tapucu's experiment[3], on the diversion cross-flow between two parallel channels communicating by a lateral slot, has shown that the lateral pressure loss coefficient is mainly a function of the ratio of the lateral flow velocity to the donor channel axial velocity, the recipient channel axial velocity, and the gap clearance and thickness of the slot. On the basis of Tapucu's experiments, Tapucu-Merilo[4] derived the axial pressure variations in terms of two new parameters for donor and recipient channels. These parameters include the combined effect of fluid transferred and drag force brought by the connection gap, and are functions of the velocities and the geometrical parameters of the slot.

Baytas[5] determined that the axial velocity in the gap region influences the cross-flow, by comparing the numerical predictions with Tapucu's experimental data. He expressed the axial velocity in the gap region in terms of the axial velocity of the adjacent channels and a new parameter, which was found by numerical optimization.

Brown et. al. [6] found that, with a constant width control volume of gap region in the subchannel approach, the results for blockage conditions could not be satisfactory. They suggested that a variable width control volume should be used to analyze the cross-flow behind the blockage.

Gencay et. al. [7] conducted the experiments for the hydraulic behavior of two laterally interconnected channels with blockages in one of them. They observed that in the upstream region of the blockage the diversion cross-flow takes place over a relatively short distance and in the downstream of the blockage the recovery of the diverted flow by the blocked channel is a slow process and the rate of this recovery decreases with increasing blockage severity. By comparing with experimental data, Tapucu et. al. [8] concluded that COBRA-IIIC may not be adequate to describe the hydrodynamic behavior of two-interconnected channels with plate type blockages much higher than 30% severity in one of them.

Gencay-Tapucu[9] defined new momentum parameters for the axial momentum equation to investigate the hydrodynamic behavior of two interconnected parallel channels when one of them has a high blockage fraction, and studied the lateral resistance between two channels by taking into account the convective contribution of transverse momentum due to axial and transverse velocities. These parameters are expressed as a function of the square of the ratio of cross-flow velocity to the donor channel velocity.

As mentioned above, many works have been performed to analyze the cross-flow mixing phenomena and develop a suitable correlation for the loss coefficient, experimentally or numerically. However, most experiments were conducted on two parallel flow channels coupled by small holes or slots, or on blowing and sucking manifolds. These seem to be quite irrelevant to nuclear fuel bundles. Also, numerical predictions are normally based on the subchannel approaches which are derived by the lumped parameter concept in the subchannel of nuclear fuel assemblies. Hence, it is required to analyze the cross-flow phenomena in more realistic situations.

In this study, a turbulent flow field analysis code in subchannels is developed, accounting for the secondary flow caused by the anisotropic feature of Reynolds stress. The numerical scheme adopted in this code is the Galerkin weighted finite element method. The code has been verified by comparing with available experimental data. Finally, using the same code, a correlation for the lateral loss coefficient between subchannels is numerically obtained in terms of the ratio of the lateral flow velocity to the donor subchannel axial velocity, recipient channel Reynolds number, and pitch-to-diameter.

2. Turbulence Model

2.1. Secondary Flow and Anisotropic Model

Turbulent flow in non-circular ducts is characterized by secondary motions in a plane perpendicular to the streamwise direction. In general, the secondary motion is caused by two different mechanisms. The pressure-induced secondary motion (of Prandtl's first kind) exists in curved ducts and its magnitude can be quite large, say of the order of 20-30% of the streamwise mean velocity. On the contrary, the secondary motion encountered in straight non-circular ducts is caused by the turbulence and thus this secondary flow can be present even under fully-developed conditions. Although the magnitude of turbulence-driven secondary motion (of Prandtl's second kind) is smaller than the root-mean-square value of turbulent intensity, this motion distorts the streamwise mean velocity and temperature contours towards the corners.

From the experimental investigations, Brundrett-Baines[10] have shown that the turbulence-driven secondary flows in non-circular ducts result from the anisotropy of Reynolds stress in the cross-sectional plane. Thus, the anisotropic Reynolds stress model should be adopted for more accurate description of the secondary flow.

The importance of anisotropic effect on the flow field in rod bundles has been confirmed by several investigations. There may be two possible ways to include the anisotropic effect in turbulence models. One is the anisotropic eddy viscosity model which accounts for the anisotropic eddy diffusion, and the other is the anisotropic algebraic Reynolds stress

model which accounts for the secondary flow.

Trupp-Aly[11] analyzed the anisotropic effect in a triangular-arrayed rod bundle by introducing a constant anisotropic factor as the ratio of eddy viscosities.

Slagter[12] developed a new form of the one-equation turbulence model allowing for the effect of anisotropic eddy viscosities. Slagter's anisotropic model is based on anisotropic length scale expressions of Carajilescov-Todreas and on Wolfshtein's length scale model which includes the damping effects near the wall and, thus, is applicable up to the wall.

Launder-Ying[13] derived the relations between the Reynolds stresses under some reasonable approximations. Using the results of order of magnitude analysis, Baker[14] established the leading terms of the Reynolds stresses which are essentially equivalent to those of the Launder-Ying model.

Myong-Kasagi[15] added some complex correction terms of second order to the isotropic Reynolds stress to describe the anisotropy and its behavior at low Reynolds number near the wall.

2.2. Low-Reynolds Number Model

Most of the turbulence models are devised for high Reynolds number and fully turbulent flows far from the wall. Thus the success of the prediction of wall-bounded shear flows depends, to a large extent, on the use of the appropriate wall functions that relate surface boundary conditions to points in the fluid away from the boundaries and thereby avoid the problem of modeling the direct influence of viscosity. However, in some cases such as subchannel analysis where the ultimate purpose is to find the rod surface temperature and informations on the flow field in the immediate vicinity of the wall is essential, the low-Reynolds number model is required.

Many low-Reynolds number models combined with widely used k-ε model were proposed[16]; Lam-Bremhorst and Launder-Sharma were the most successful in using this approach. Especially, the Lam-Bremhorst model has the advantage in that it does not require additional terms to the standard k-ε model.

3. Mathematical Model

In this study, a two-dimensional turbulent model including the secondary flow calculation has been established to obtain an analytical correlation of the lateral pressure loss coefficient between subchannels based on detailed knowledge of the velocity field in such domain. In the analysis, instead of the lumped parameter concept, the field equations are solved directly. In order to obtain the amount of cross-flow between square-arrayed subchannels, mass and momentum conservation equations were written under the steady state and fully-developed conditions.

The low-Reynolds number k-ε model suggested by Lam-Bremhorst[17] is used to describe the complex turbulent phenomena near the wall. Thus, instead of the wall function, the no-slip wall boundary condition is used. This means that with this approach the velocity and the temperature profiles, even in the vicinity of the wall, can be calculated. The anisotropic Reynolds stress model of Launder-Ying is adopted for more accurate description on the secondary flow. Although the Launder-Ying model was developed for the fully turbulent region and the constants were adjusted to the square duct geometry, Lee et. al. [18] applied this model up to the wall successfully for the closely-packed rod array (P/D = 1.123). However, it was found that the larger pitch-to-diameter, the more discrepancy between the predicted values and the experimental data resulted. So, in this study, the model constant was modified to take into consideration the aspect ratio (pitch-to-diameter) through a numerical optimization.

The continuity equation and transverse direction momentum equations are transformed into vorticity and stream functions to construct the convenient and

efficient numerical scheme. The Galerkin weighted residual finite element method is used to solve the governing equations effectively.

3.1. Governing Equations

The governing equations for the analysis of the flow field in subchannels are established as follows and, for simplicity, the Cartesian tensor notations are used; the subscripts i and j denote lateral coordinates 1 and 2, respectively.

- Stream function

$$U_1 = \frac{\partial \Psi}{\partial x_2}, \quad U_2 = -\frac{\partial \Psi}{\partial x_1} \tag{1}$$

- Axial vorticity

$$\Omega = \frac{\partial U_2}{\partial x_1} - \frac{\partial U_1}{\partial x_2} \tag{2}$$

- Stream function equation

$$\frac{\partial^2 \Psi}{\partial x_j \partial x_j} = -\Omega \tag{3}$$

- Axial momentum equation

$$U_j \frac{\partial U_3}{\partial x_j} - \frac{\partial}{\partial x_j}\left((\nu + \nu_T)\frac{\partial U_3}{\partial x_j}\right) = -\frac{1}{\rho}\frac{\partial P}{\partial x_3} \tag{4}$$

- Axial vorticity equation

$$\frac{\partial}{\partial x_j}\left(\Omega U_j + \overline{\omega u_j} - \nu \frac{\partial \Omega}{\partial x_j}\right) = 0 \tag{5}$$

- Turbulent kinetic energy equation (k equation)

$$U_j \frac{\partial k}{\partial x_j} - \frac{\partial}{\partial x_j}\left((\nu + \nu_T/\sigma_k)\frac{\partial k}{\partial x_j}\right) = P_k - \varepsilon, \tag{6}$$

$$P_k = -\overline{u_1 u_3}\frac{\partial U_3}{\partial x_1} - \overline{u_2 u_3}\frac{\partial U_3}{\partial x_2},$$

$$\nu_T = C_\mu f_\mu \frac{k^2}{\varepsilon},$$

$$f_\mu = (1 - \exp(-B_\mu R))^2 \left(1 + \frac{D_\mu}{R_t}\right),$$

$$R = \frac{k^{1/2} x_l}{\nu}, \qquad R_t = \frac{k^2}{\varepsilon \nu}$$

where

$\sigma_k = 1.0$, $B_\mu = 0.0165$, $C_\mu = 0.09$, $D_\mu = 20.5$

- Turbulent kinetic energy dissipation rate equation (ε equation)

$$U_j \frac{\partial \varepsilon}{\partial x_j} - \frac{\partial}{\partial x_j}\left((\nu + \nu_T/\sigma_\varepsilon)\frac{\partial \varepsilon}{\partial x_j}\right) = C_{\varepsilon 1} f_{\varepsilon 1} \frac{\varepsilon}{k} P_k - C_{\varepsilon 2} f_{\varepsilon 2} \frac{\varepsilon^2}{k}, \tag{7}$$

$$f_{\varepsilon 1} = 1 + \left(\frac{A_{\varepsilon 1}}{f_\mu}\right)^3, \quad f_{\varepsilon 2} = 1 - \exp(-R_t^2)$$

where

$\sigma_\varepsilon = 1.3$, $A_{\varepsilon 1} = 0.05$, $C_{\varepsilon 1} = 1.44$, $C_{\varepsilon 2} = 1.92$

- Pressure equation

$$\frac{\partial^2}{\partial x_i \partial x_j}\left(U_i U_j + \overline{u_i u_j} + \frac{P}{\rho}\delta_{ij}\right) = 0 \tag{8}$$

- Anisotropic algebraic Reynolds stresses

$$-\overline{u_i u_3} = \nu_T \frac{\partial U_3}{\partial x_i} \tag{9}$$

$$-\overline{u_i u_j} = C_3 k \delta_{ij} - C \frac{k^3}{\varepsilon^2}\frac{\partial U_3}{\partial x_i}\frac{\partial U_3}{\partial x_j} \tag{10}$$

where

$C = -0.00237(P/D - 1) + 0.000871$, $C_3 = 0.562$

As mentioned above, the model constant C was adjusted satisfy both equilateral triangular and square-arrayed rod bundle geometries.

3.2. Boundary Conditions

The boundaries of the subject domain consist of rod surface, symmetry boundary, and inflow and outflow boundaries, which permit flow-in and flow-out causing the cross-flow between adjacent two subchannels. Thus, three types of boundary conditions are needed; no-slip condition on the rod surface, symmetry condition on the symmetry boundary, and inlet and outlet conditions on the inflow and outflow boundaries.

On the rod surface, all components of the velocit-

ies and turbulent kinetic energy are zero from the no-slip condition and the stream functions can also be set to zero. However, for the axial vorticity and dissipation rate of turbulent kinetic energy, the boundary conditions are neither exact nor simple. Furthermore, some of them, even used commonly, are likely to cause the divergence of solutions especially at high Reynolds number[19]. Thus, in this study, new types of wall conditions of third order are derived, with the Taylor expansion and the near wall behavior of turbulence and under the assumption that the length of the first and the second grid are equal, as follows;

$$\Omega_w = \frac{\Psi_{w+1}}{0.5\,\Psi_{w+2} - \Psi_{w+1}}\,\Omega_{w+1}\,, \qquad (11)$$

$$\varepsilon_w = \frac{3\,k_{w+1}}{k_{w+2} - k_{w+1}}\,\varepsilon_{w+1}\,. \qquad (12)$$

On the symmetry boundaries, the normal gradients of axial velocity, turbulent kinetic energy and its dissipation rate and vorticity are set to zero. On the other hand, the stream function is equal to zero on the stream line containing the rod surface and on the symmetry line it can be calculated from the inlet and outlet flowrates.

If it is assumed that the normal fluxes of all physical quantities of the inflow and outflow are zero, the normal gradients of these quantities are zero along the inlet and outlet boundaries. And, the stream function and axial vorticity can be calculated from the velocity distribution along these boundaries.

3.3. Numerical Scheme

The governing equations were formulated numerically by the Galerkin weighted residual finite element method using bilinear cardinal bases satisfying the C^0 continuity[14]. The two dimensional calculation domain was discretized into square finite elements.

In general, numerical analyses on turbulent flows suffer from severe non-linearity and numerical instability. Thus, the initial guesses of dependent variables, mesh spacing and iteration scheme must be determined carefully. Initial profiles of the axial velocity, turbulent kinetic energy and its dissipation rate were obtained by universal profiles. The universal velocity profile was also used to determine the mesh spacing. To filter the oscillatory behavior of numerical solutions, the guessed values for the next iteration were obtained by using the geometric mean of the value of the previous iteration step and the calculated value with an under-relaxation factor.

The convergence criteria used was that the maximum individual relative error should be below 10^{-3} except for the stream function and axial vorticity for which the criteria recommended by Gosman et. al. [20] was applied.

All of the governing equations were not solved simultaneously, but segregatedly. The equations were divided into two groups, the first consisted of the axial momentum, turbulent kinetic energy and its dissipation rate equation and the second included the axial vorticity and stream function equations. Each group formed an independent iteration set, in which each equation was solved by an inner iteration procedure. The pressure distribution was found after the solutions of the five dependent variables met the con vergence criteria.

4. Results and Discussion

The calculations of the flow field in domains such as shown in Figs. 1 and 2 have been implemented using the turbulent model described above. In order to validate this model, the predicted distributions of axial velocities and stream functions under various geometrical and hydraulical conditions were compared with well-known experimental data.

Figs. 3 and 5 show the comparison of the computed axial velocity contours with experimental results on a triangular array[21] of P/D=1.123 and Re=27,000 and on a square array[22] of P/D=1.25 and Re=100,000, respectively. The first result shows a good agreement but the second deviates

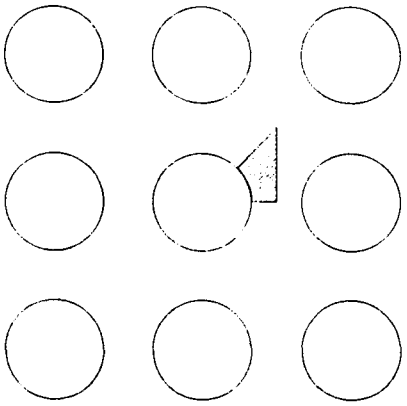

Fig. 1. Unit Subchannel of Square rod Bundle Array

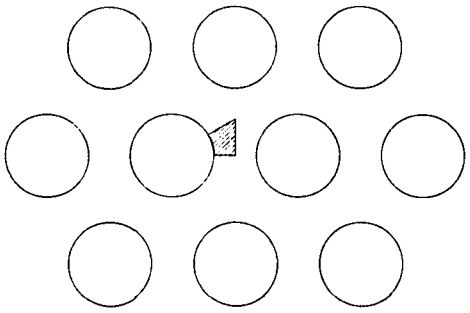

Fig. 2. Unit Subchannel of Triangluar rod Bundle Array

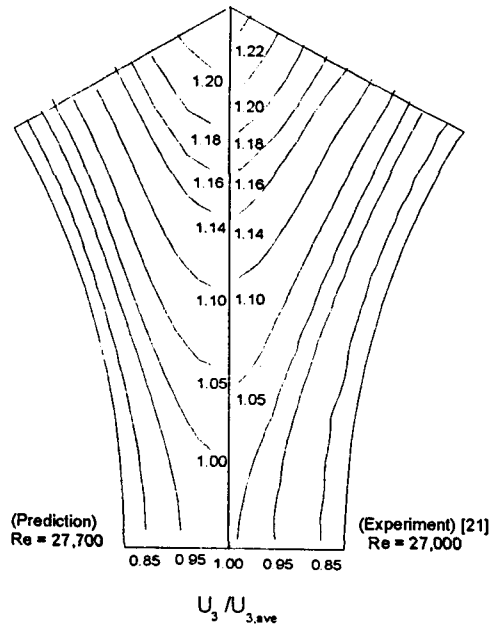

Fig. 3. Axial Velocity Contour With Secondary Flow in a Triangular Subchannel (P/D=1.123)

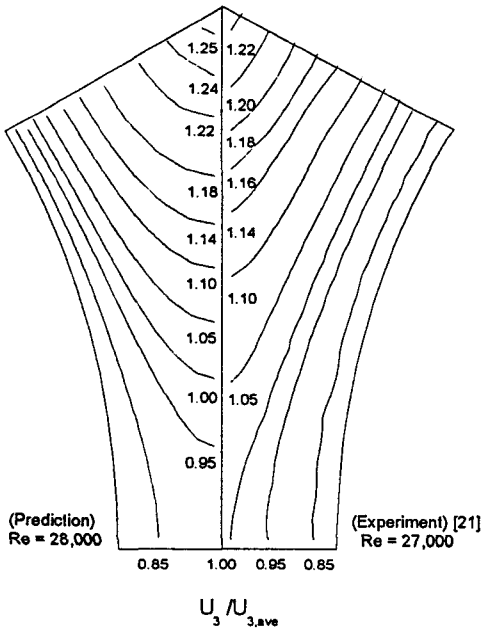

Fig. 4. Axial Velocity Contour Without Secondary Flow in a Triangular Subchannel (P/D=1.123)

from the experimental data slightly. However, the difference is within 5% on the basis of maximum velocity. Predictions without secondary flow are shown in Fig. 4. It shows that the secondary flow makes uniform flow field with convective transport from the core to the gap region. Fig. 6 shows that the wall shear stress distribution in triangular array.

Carajilescov-Todreas[21] failed to measure the secondary flow velocities in the equilateral triangular arrays but predicted the result of the existence of two swirls in a unit cell. They insisted that the weaker swirl be almost vanished for P/D=1.217. However,

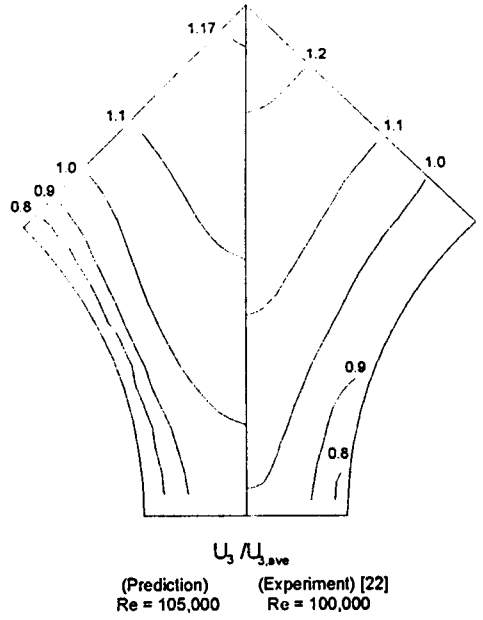

Fig. 5. Axial Velocity Contour in a Square Subchannel (P/D=1.25)

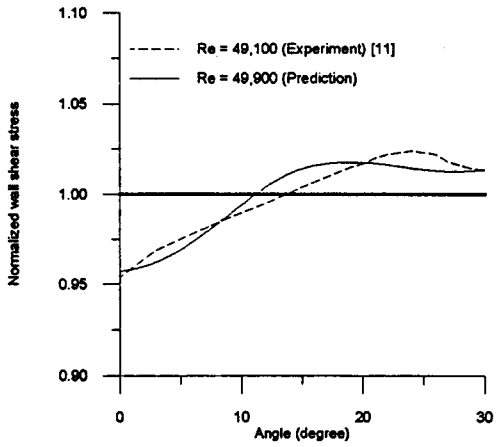

Fig. 6. Wall Shear Distribution in a Triangular Subchannel (P/D=1.20)

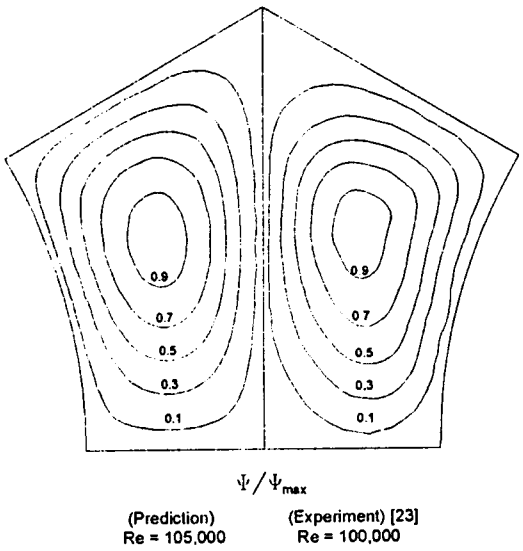

Fig. 7. Streamline in a Triangular Subchannel (P/D=1.30)

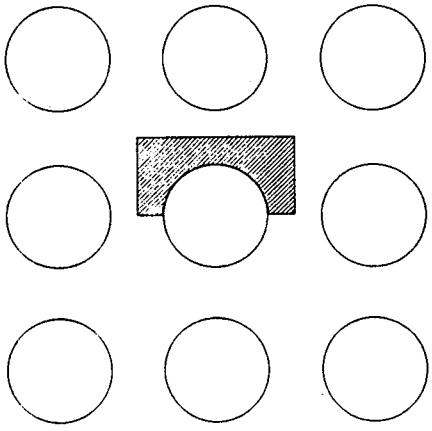

Fig. 8. Calculation Domain for Cross-flow in Square Rod Bundle Array

Trupp-Aly[11] found a single swirl of secondary flow from the numerical analysis. Vonka[23] measured the secondary flow velocities successfully and observed only a single swirl. In this analysis, a single swirl was obtained not only for the equilateral triangular array but also for the square array. Fig. 7 shows the predicted and experimentally measured stream lines under the condition of P/D = 1.30 and Re = 100,000

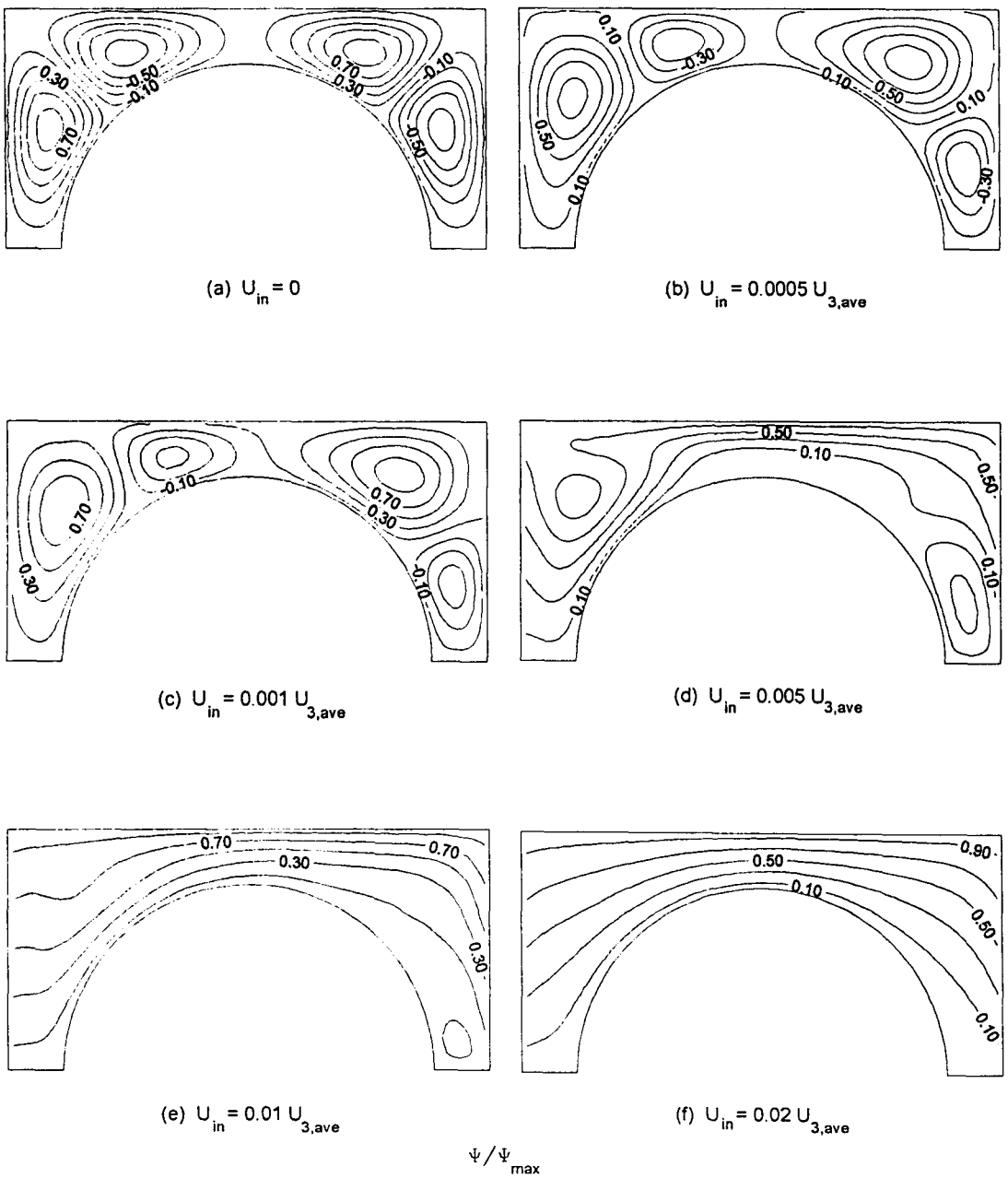

Fig. 9. Cross-flow Streamline Variations (P/D=1.30, Re=100,000)

for the equilateral triangular array.

For the analysis of the cross-flow, the next step is to calculate the flow field composed of 4 unit cells such as Fig. 8 with the verified model. The upper and lower boundaries are assumed to be symmetrical. The left and right are flow-inlet and outlet, respectively; equal amounts of mass flow in and out cause the cross-flow, without violation of the fully-developed condition.

Predictions of the streamlines under the various inlet flowrate conditions are shown in Fig. 9. This figure shows that the swirl of the secondary flow almost vanishes when the ratio of the inlet flow velocity to the axial velocity is greater than 1%.

To construct the correlation, many calculations were performed, varying P/D = 1.15 − 1.30, Re = 50,000 − 100,000 and the ratio of cross-flow velocity to axial velocity up to 5.4%. Once the distributions of flow variables such as velocity and pressure in the flow field are determined through the numerical analysis, the lateral loss coefficient K can be obtained,

$$K = \frac{\Delta P}{\frac{1}{2}\rho U_{cross}^2} , \qquad (13)$$

where the difference between channel-averaged pressures can be calculated from the pressure distribution in each channel. Fig. 10 shows the distribution of lateral loss coefficients, which are decreasing exponentially as the ratio of the cross-flow velocity to the axial velocity of donor subchannel, U_{cross}/U_{don}, increases. It also implies that the ratio of U_{cross}/U_{don} is a cruicial parameter on the lateral loss coefficient. On the other hand, for P/D smaller than about 1.23, K decreases with P/D. However, for larger P/D, K increases.

A correlation for K was constructed in terms of U_{cross}/U_{don}, Reynolds number based on the axial velocity of recipient subchannel, Re_{rec}, and P/D according to the proposition of Tapucu[3];

$$K = 32.8\, K_{P/D} K_{rec} \exp(-156 \frac{U_{cross}}{U_{don}}) \qquad (14)$$

where

$$K_{P/D} = 32.4(P/D - 1)^2 - 15.1(P/D - 1) + 2.68 ,$$

$$K_{rec} = 1.79 - 1.03 \frac{Re_{rec}}{10^5} .$$

Fig. 11 shows the correlation diagram.

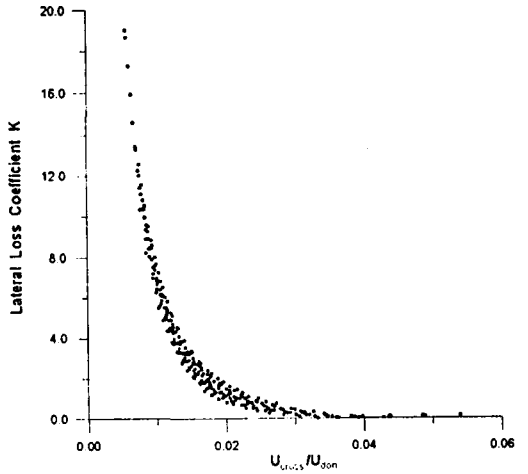

Fig. 10. Distribution of the Calculated Lateral Loss Coefficient

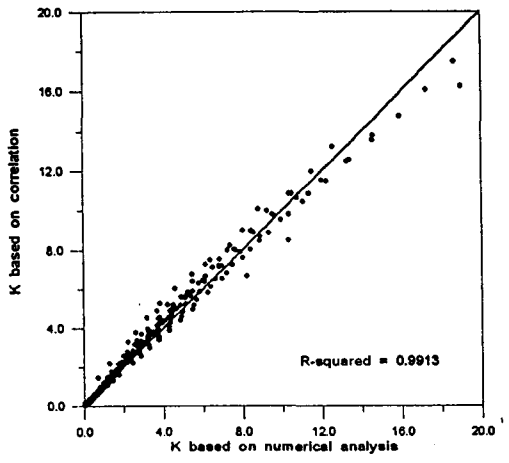

Fig. 11. Correlation Diagram of Lateral Loss Coefficient

5. Conclusions

The nuclear subchannel analysis codes such as COBRA and TORC for reactor design and safety analysis use the lateral pressure loss coefficient to predict the cross-flow between subchannels. In this study, a computer code for two-dimensional fully-developed turbulent flow fields was developed to predict the analytical lateral loss coefficient correlation. The model in the code includes the secondary flow, anisotropic algebraic Reynolds stress of Lander-Ying and low-Reynolds number k-ε model. Launder-Ying's model constant was also modified through the numerical optimization to be suitable to the rod bundle geometry.

For the code verification, the numerical results for a unit cell were compared with experimental data and the predictions were shown to be in satisfactory agreements. A large number of calculations were performed under the various geometrical and hydraulical conditions to find the lateral loss coefficients; a numerical correlation was also determined. This correlation is on the form of a function of the ratio of the lateral flow velocity to the donor subchannel axial velocity, recipient channel Reynolds number, and pitch-to-diameter. In addition, it is expected that the model developed in this study, which can predict an accurate velocity field in subchannels, may be applied in the future to calculate the temperature distribution and other subchannel parameters analytically.

Table of Nomenclature

k turblent kinetic energy($=\overline{u_iu_i}/2$)
K lateral pressure loss coefficient
P pressure
P/D pitch-to-diameter
Re Reynolds number
U_i mean velocity of i direction
u_i velocity fluctuation of i direction
$\overline{u_iu_j}$ Reynolds stress
x_i coordinate of i direction
x_1 normal distance from the wall
δ_{ij} Kronecker delta
ε dissipation rate of turbulent kinetic energy
ν molecular kinematic viscosity
ν_T eddy viscosity
ρ density
Ψ stream function
Ω mean axial vorticity
ω axial vorticity fluctuation
$\overline{\omega u_i}$ correlation between axial vorticity fluctuation and velocity fluctuation

Subscript

ave average value
i, j Cartesian index (3 for axial direction)
cross cross-flow
don donor channel
rec recipient channel
w wall

Acknowledgement

This work has been supported in part by Electrical Engineering & Science Research Institute grant, 93-41 which is funded by Korea Electric Power Co.

References

1. J.H. Rust, *Nuclear Power Plant Engineering*, Haralson Publishing Company (1979)
2. J. Weisman, "Cross flow resistance in rod bundle cores," *Nucl. Tech.*, 15, pp. 465-469 (1972)
3. A. Tapucu, "Studies on diversion cross-flow between two parallel channels communicating by a lateral slot I : Transverse flow resistance coefficient," *Nucl. Engrg. Des.*, **42,** pp. 297−306 (1977)
4. A. Tapucu and M. Merilo, "Studies on diversion cross-flow between two parallel channels communicating by a lateral slot II : Axial pressure var-

iations," *Nucl. Engrg. Des.*, **42,** pp. 307−318 (1977)

5. A.C. Baytas, "A comparison of prediction and Tapucu experimental data for determination of the axial velocity in the gap region," *Nucl. Tech.*, **90,** pp. 417−425 (1990)
6. W.D. Brown, E.U. Khan, and N.E. Todreas, "Prediction of cross flow due to coolant channel blockage," *Nucl. Sci. Eng.*, **57,** pp. 164−174 (1975)
7. S. Gencay, A. Tapucu, N. Troche, and M. Merilo, "Experimental study of the diversion crossflow caused by subchannel blockages. Part I : Experimental procedure and mass flow rates in the channels," *J. Fluids Engrg.*, **106,** pp. 435−440 (1984)
8. A. Tapucu, S. Gencay, N. Troche, and M. Merilo, "Experimental study of the diversion crossflow caused by subchannel blockages. Part II : Pressures on the channels and the comparison of the COBRA-IIIC predictions with experimental data," *J. Fluids Engrg.*, **106,** pp. 441−447 (1984)
9. S. Gencay and A. Tapucu, "Cross-flow between identical subchannels caused by severe blockage," *Nucl. Engrg. Des.*, **127,** pp. 33−45 (1991)
10. E. Brundrett and W. D. Baines, "The Production and diffusion of vorticity in duct flow," *J. Fluid Mech.*, **19,** pp. 375−394 (1964)
11. A.C. Trupp and A.M.M. Aly, "Predicted secondary flows in triangular array rod bundles," *J. Fluids Engrg.*, **101,** pp. 354−363 (1979)
12. W. Slagter, "Finite element solution of axial turbulent flow in a Bare rod bundle using a one-equation turbulence model," Nucl. Sci. Eng., 82, pp. 243−259 (1982)
13. B.E. Launder and W.M. Ying, "Prediction of flow and heat transfer in ducts of square cross-section," *Proc. Instn. Mech. Engrs.*, **187,** pp. 455−461 (1973)
14. A.J. Baker, *Finite Element Computational Fluid Mechanics,* McGraw Hill Book Company (1985)
15. H.K. Myong and N. Kasagi, "Prediction of the near-wall turbulence with an anisotropic low-Reynolds-number k-ε turbulence model," *J. Fluids Engrg.*, **112,** pp. 521−524 (1990)
16. V.C. Patel, W. Rodi, and G. Scheuerer, "Turbulence models for near-wall and low Reynolds number flow: A review," *AIAA J.*, **23,** pp. 1308−1319 (1984)
17. C.K.G. Lam and K. Bremhorst, "A modified form of the k-ε model for predicting wall turbulence," *J. Fluids Engrg.*, **103,** pp. 456−460 (1981)
18. K.B. Lee, H.C. Jang, and S.K. Lee, "Study of the secondary flow effect on the turbulent flow characteristics in fuel rod bundles," *J. KNS*, **26,** pp. 345−354 (1994)
19. P.J. Roache, *Computational Fluid Dynamics,* Hermosa Publishers (1972).
20. A.D. Gosman, W.M. Pun, A.K. Runchal, D.B. Spalding, and M. Wolfshtein, *Heat and Mass Transfer in Recirculating Flows,* Academic Press (1969)
21. P. Carajilescov and N.E. Todreas, "Experimental and analytical study of axial turbulent flows in an interior subchannel of a bare rod bundle," *J. Heat Transfer,* **93,** pp. 262−268 (1976)
22. A.S. Yang and C.C. Chieng, "Turbulent heat and momentum transports in an infinite rod array," *J. Heat Transfer,* **109,** pp. 599−605 (1987)
23. V. Vonka, "Measurement of secondary flow vortices in a rod bundle," *Nucl. Engrg. Des.*, **106,** pp. 191−207 (1988)